



NOVA

University of Newcastle Research Online

nova.newcastle.edu.au

Sweeney, James; Webber, Grant B.; Rutland, Mark W.; Atkin, Rob 'Effect of ion structure on nanoscale friction in protic ionic liquids ', Physical Chemistry Chemical Physics Vol. 16, Issue 31, p. 16651-16658 (2014)

Available from: <http://dx.doi.org/10.1039/c4cp02320j>

Accessed from: <http://hdl.handle.net/1959.13/1046450>

Effect of Ion Structure on Nanoscale Friction in Protic Ionic Liquids

James Sweeney¹, Grant B. Webber¹, Mark W. Rutland^{2,3}, Rob Atkin^{1,*}

¹Centre for Advanced Particle Processing and Transport, Newcastle Institute for Energy and Resources, The University of Newcastle, Callaghan, NSW 2308, Australia

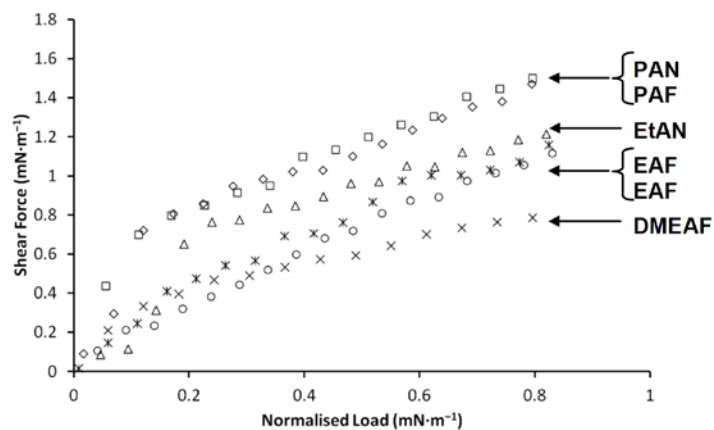
²Surface and Corrosion Science, Department of Chemistry, Royal Institute of Technology, SE-100 44 Stockholm, Sweden

³SP Technical Research Institute of Sweden, Stockholm, Sweden

* To whom correspondence should be addressed.

Email: rob.atkin@newcastle.edu.au

Graphical Abstract



Abstract

The effect of ionic liquid (IL) molecular structure on nanoscale friction has been investigated using colloidal probe Friction Force Microscopy (FFM). The ILs studied were ethylammonium formate (EAF), ethylammonium nitrate (EAN), propylammonium formate (PAF), propylammonium nitrate (PAN), dimethylethylammonium formate (DMEAF), and ethanolammonium nitrate (EtAN). ILs were confined between a silica colloid probe and a mica surface, and the friction force was measured as a function of normal load for sliding velocities between 10 and 40 $\mu\text{m}\cdot\text{s}^{-1}$. At low normal forces, multiple IL layers are found between the probe and the surface, but at higher force, in the boundary layer regime, a single ion layer separates the probe and the surface. In the boundary layer regime energy is dissipated by two main pathways. Firstly, the ionic liquid near the surface, with the exception of the boundary layer, is expelled from the advancing contact made by the probe on the surface. This disruption in the interactions between the boundary layer and the near surface multilayers, leads to energy dissipation and depends on the strength of the attraction between the boundary and near surface layers,. The second pathway is via rotations and twists of ions in the boundary layer, primarily associated with the cation terminal methyl group. The friction coefficient did not vary over the limited range of sliding speeds investigated

Introduction

Ionic liquids (ILs) are pure salts with melting points less than 100 °C. They generally consist of large, asymmetric organic cations, with few constraints on the nature or size of the anions. Melting points are reduced compared to conventional salts due to steric interactions which weaken Columbic interactions and prevent packing into crystal lattice structures. The charge is furthermore delocalised over the ion, further weakening Columbic interactions.¹ ILs may be classified as either protic or aprotic depending on the method of synthesis; protic ILs are formed by proton transfer from a Brønsted-Lowry acid to a Brønsted-Lowry base, while aprotic ILs are formed by charge-transfer metathesis and quaternisation reactions.

The physicochemical properties of ILs are functions of their ionic structures. ILs have been dubbed “designer” solvents because it is possible to tailor ILs at the molecular level, to achieve the appropriate properties for a given application.² Certain desirable properties are common to a large number of ILs, such as low vapour pressure, high thermal stability, large electrochemical windows, reasonable thermal conductivity, and the ability to solubilise a large range of solutes. Consequently, ILs have generated a large amount of research interest over the past two decades³⁻⁶ in fields spanning catalysis,⁷ particle stability,⁸ electrodeposition,⁹ phenomena occurring at solid-liquid^{10, 11} and liquid-air interfaces,^{12, 13} and electrochemistry where ILs have been used as electrolytes for batteries¹⁴ and for dye-sensitised solar cells.¹⁵ ILs have also been used as solvents for surfactant self-assembly,¹⁶⁻²⁰ in carbon dioxide capture and sequestration,²¹ and as lubricants for mechanical parts.²²⁻³³

In the latter application the primary benefits come from the low vapour pressure and high thermal stability, but ILs are also electrical conductors so can be used to lubricate electrical contacts unlike conventional lubricants which are often insulators. Certain ILs have been shown to have superior friction reduction and anti-wear properties compared to conventional

high performance synthetic organic lubricants such as perfluoropolyethers (PFPEs),³⁴⁻³⁸ and many ILs are cheaper than PFPEs.³⁹

Protic ILs have distinct bulk nanostructure.⁴⁰⁻⁴³ Except for dimethylethylammonium formate (DMEAF), the ILs investigated in this study are known to have sponge like morphologies.^{40, 41, 43} The bulk structure of (DMEAF) has not been reported to the authors' knowledge. However, bulk and interfacial nanostructure are known to be closely related,² and DMEAF is much more weakly structured near a mica surface than the other ILs.¹¹ This is likely a consequence of the relatively bulky cations hindering efficient packing. It is likely that DMEAF is weakly structured in the bulk.

At a solid interface, the near surface IL ions align into layers. The strong near surface layered structure decays to the bulk sponge morphology over a distance of several nanometres normal from the surface.⁴⁰ Surface Force Apparatus (SFA)⁴⁴⁻⁴⁸ and Atomic Force Microscopy (AFM)^{3, 4, 10, 11, 44, 49, 50} experiments have shown strong interfacial layering in a wide range of IL systems. Previous AFM experiments with ethylammonium nitrate (EAN)⁵¹ and propyl ammonium nitrate (PAN)⁵² on mica have shown that the ion layer in contact with the substrate consists of cations electrostatically adsorbed to the mica surface *via* their ammonium headgroups. Additional "solvophobically" adsorbed cations are also adsorbed to the surface, occupying spaces between electrostatically adsorbed cations. This is driven by the need to satisfy attractive solvophobic interactions between alkyl chains. (Solvophobic interactions are analogous to hydrophobic interactions in water.⁵³) Anions are adsorbed into the surface layer to neutralise the charge of each solvophobically adsorbed cation; the interfacial boundary ion layer consists of electrostatically bound cations, and solvophobically adsorbed cations with associated anions to preserve electroneutrality.

In this study Friction Force Microscopy (FFM) is used to study the shear force as a function of normal load and sliding velocity for the ILs ethylammonium formate (EAF), EAN, propylammonium formate (PAF), PAN, DMEAF, and ethanolammonium nitrate (EtAN). Due to their water sensitivity protic ILs are unlikely to be used in real world lubrication applications. However, because their chemical structures can be systematically fine-tuned, this enables the different dissipation pathways to friction to be commented upon, making protic ILs well suited to fundamental studies. At low force, multiple ion layers are between the surfaces, and the friction force is very low. The primary focus of this paper is the “boundary regime”, which occurs at higher normal loads, when only a single layer of ions remain between the surfaces.⁵⁴ Under this condition it is possible to elucidate the relationship between molecular-scale energy dissipation phenomena, such as ion conformation changes, and the friction responses of each IL.

Friction results from energy dissipation while sliding. Energy can be dissipated by a boundary layer through a variety of pathways. Many of these are also available to (structurally similar) self-assembled monolayers (SAMs), while others are IL-centric. These dissipation pathways include bond rotations and stretches,⁵⁵ disruption of intermolecular interactions such as hydrogen bonds and van der Waals (vdW's) forces,^{56, 57} ion adsorption and desorption from the boundary layer,^{45, 52, 54} and changes to conformations of ions.^{55, 57-61} Conformational changes are more prevalent for loosely packed layers, like those formed when alkyl chains are terminated by bulky terminal groups, or when gauche deformations occur.^{55, 57, 58} For example, a terminal gauche defect shortens the chain by $\approx 1 \text{ \AA}$ and disrupts packing arrangements. This weakens intermolecular interactions⁵⁵ and further conformation changes are more likely to occur, leading to higher friction.⁶²

Dissipation pathways are often interrelated; packing density is a function of the strength of vdW's interactions, which is influenced by alkyl chain length. For SAMs, friction decreases

as alkyl chain length is increased due to stronger lateral vdW's forces.^{57, 62, 63} Strong vdW's forces between long alkyl chains produce densely packed, (relatively) defect free, monolayers. The absence of defects means the monolayers are well ordered, so few excitation modes are available and friction is low.

Materials and Methods

Nitrate ILs were prepared by drop-wise addition of equimolar quantities of nitric acid (RCI Labscan Ltd., Thailand, 70% w/w aqueous solution) to the appropriate amine; ethylamine (Sigma-Aldrich, USA, 66-72% w/w aqueous solution), propylamine (Sigma-Aldrich, Germany, $\geq 99.0\%$ purity), or ethanolamine (Sigma-Aldrich, USA, $\geq 99\%$ purity). Formate ILs were prepared by drop-wise addition of formic acid (Sigma-Aldrich, Germany, $\sim 98\%$ purity) to the appropriate amine; ethylamine, propylamine, or dimethylethylamine (Sigma-Aldrich, Germany, 99% purity). The solutions were maintained at 8 – 10 °C to prevent the formation of oxide impurities.

Excess water was removed by rotary evaporation. Nitrate ILs were then heated to 100 – 110 °C under a nitrogen atmosphere for approximately 12 hours to reduce the water content further. Formate ILs were not heated to prevent the formation of amides.⁶⁴ Instead, a high vacuum pump (Brook Crompton Betts, Australia) attached to a liquid nitrogen trap was used. Nitrate ILs had water content of less than 0.1 wt%, and formate ILs less than 0.5 wt%, as determined by Karl-Fischer titration.

Normal force curves were obtained with a Nanoscope IV MultiMode AFM (Bruker, Santa Barbara, California) equipped with a PicoForce controller and scanner in contact mode. Scan rates from 0.015 to 0.1 Hz were used with scan sizes from 30 to 100 nm. Shear force *vs.* normal load data were obtained with the same AFM. The scan angle was set to 90° and the slow scan axis was disabled. Scan rates from 0.5 Hz to 3.95 Hz were used with a scan size of

5 μm . Shear force was measured as a function of normal load for normalised loads from 0 $\text{mN}\cdot\text{m}^{-1}$ to approximately 1 $\text{mN}\cdot\text{m}^{-1}$. The normal load was increased to its maximum value and then decreased until the tip became fully retracted (adhesion in the systems tested was minimal, so this usually occurred at a normal load close to 0 nN). Each point on the shear force vs. normal load plots is an average of three separate experiments, where each data point was calculated from sixteen forwards (trace) and backwards (retrace) motions of the colloid probe over the same line on the surface. The lateral deflection of the cantilever was converted into shear force using a custom built MATLAB 7.11.0 function. The lateral deflection sensitivity was calibrated using the methods of Liu *et al.*,⁶⁵ and Schwartz *et al.*⁶⁶ The standard deviation of the lateral force data was less than 15% of the average value for most data; the low force regime was noisier for all ILs, and the data for PAF also had greater error. Friction coefficients were calculated by fitting a straight line to the low and high normal force regions, respectively, and the R^2 values of these fits were always greater than 0.95.

The IL was contained in a fluid cell sealed with a silicone O-ring, both of which were rinsed prior to use with reverse osmosis water and distilled ethanol and then allowed to dry. An atomically smooth muscovite mica surface was prepared by cleaving along the basal plane using adhesive tape.

The flexural resonant frequencies and Q-factors of tipless *n*-type silicon cantilevers (model CSC12, MikroMasch, Tallinn, Estonia) were measured using the cantilever tune function of the Tapping Mode Nanoscope AFM software. Cantilevers were imaged using an optical microscope (Zeiss, Axioskop 40) with built-in camera (Zeiss, AxioCam Cc1). Cantilever dimensions, and the diameters of colloid probes^{67, 68} (see below) were measured using AxioVision software (Zeiss, AxioVision 4.7). The normal⁶⁹ and torsional⁷⁰ spring constants of the cantilevers were determined using the Sader method. A two part epoxy (Selley's Super Strength Araldite) was used to glue borosilicate colloid probes (Duke Scientific, Palo Alto,

CA) with nominal diameters of $14.5 \mu\text{m}$. Prior to an experiment, the cantilever was rinsed with reverse osmosis water and distilled ethanol and then irradiated with UV/ozone radiation for approximately 5 minutes to remove organic residues. The same cantilever and colloid probe combination was used for all data collected in this study which enables direct comparison of data sets. Normal and shear forces have both been normalised by $2\pi R$, where R is the radius of the colloid probe in accordance with the Derjaguin approximation.⁷¹ The results in this study are reproducible as verified from experiments involving at least two separate AFM set-ups. During each experimental set-up three loading-unloading cycles were performed at each of the five sliding velocities studied. The shear forces displayed represent the average shear force from at least three repeat loading and unloading cycles on different days.

Results and Discussion

The effect of protic IL ion structure on friction at one sliding velocity is described first. In this context the influence of sliding velocity on lubricity is then examined.

Shear force as a function of normal load for the protic ILs at a sliding velocity of $40 \mu\text{m}\cdot\text{s}^{-1}$ is shown in Figure 1. Over several studies we have shown that when the apparent separation is zero for these IL systems the AFM probe is in contact with a layer of ions strongly bound to the substrate (the boundary layer) and not in contact with the surface.^{11, 51, 52, 72}

Two friction regimes are apparent in Figure 1: the low normal force *multilayer regime*, where there are multiple ion layers separating the probe and the surface, and the *boundary regime*, where the colloid probe slides against the boundary layer. The normal load delineating the transition from the multilayer regime to the boundary regime is that associated with the final step in the normal force curve, when the compliance region is reached.^{52, 54} All of the ILs

investigated here are in the boundary regime when the normal load is greater than 0.2 $\text{mN}\cdot\text{m}^{-1}$ (c.f. Figure 2, and the Supporting Information Figures A to F).

In the boundary regime, the lateral force increases in the order $\text{DMEAF} < \text{EAF} \approx \text{EAN} < \text{EtAN} < \text{PAN} \approx \text{PAF}$. This order, and the approximate differences in magnitude between the shear forces, is consistent for all sliding velocities as shown in Figures G to J of the Supporting Information. Friction coefficients for the $40 \mu\text{m}\cdot\text{s}^{-1}$ sliding velocity in the multilayer regime and the boundary regime (calculated over the normal load range from 0.2 $\text{mN}\cdot\text{m}^{-1}$ to 1 $\text{mN}\cdot\text{m}^{-1}$) are presented in Table 1.

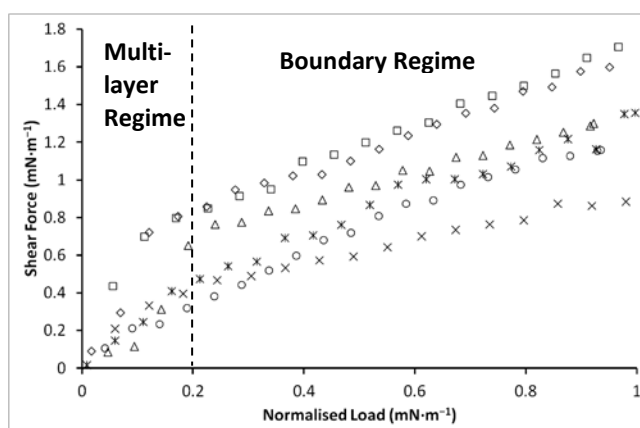


Figure 1. Shear force as a function of normal load at a sliding velocity of $40 \mu\text{m}\cdot\text{s}^{-1}$ for each IL in this study. The shear force presented is the average of at least three normalised datasets taken with the same cantilever/colloidal probe combination. Squares: PAF, diamonds: PAN, triangles: EtAN, stars: EAN, circles: EAF, crosses: DMEAF.

Table 1. Friction coefficients for each IL used in this study at a sliding velocity of $40 \mu\text{m}\cdot\text{s}^{-1}$. Friction coefficients are evaluated in the boundary regime; they are for normal loads from 0.2 $\text{mN}\cdot\text{m}^{-1}$ to 1.0 $\text{mN}\cdot\text{m}^{-1}$.

Protic IL	Multilayer Regime Friction Coefficient, μ	Boundary Regime Friction Coefficient, μ
PAN	4.4	1.1
PAF	4.5	1.1
EtAN	2.9	0.8
DMEAF	2.2	0.6
EAN	2.3	1.1
EAF	1.7	1.1

For all the protic ILs except EAF the lateral force rises sharply in the multilayer regime (higher effective friction coefficient)⁵² and then more gently at higher force in the boundary layer regime (lower friction coefficient). The friction coefficients for both regimes are shown in Table 1. The behaviour of EAN has been described in a previous manuscript,⁵⁴ so will not be discussed in detail here; new data for EAN is shown for comparison. Nanotribological experiments such as these often show non-linear behaviour due to changes in contact area, and these can be approximated using simple contact mechanics. We do not believe this is the case here. Our group,^{23,54} and others using dissimilar geometries,⁴⁵ have previously demonstrated the friction in IL systems is dependent on the number of layer trapped between the sliding surfaces. Additionally, the magnitude of the friction in the multilayer regime is dependent on both the applied load and sliding speed, which is not true for a contact mechanical approach. Finally, contact mechanics would predict a smooth transition from a power law to a linear relationship, not the abrupt change observed here.

The magnitudes of the friction *force* for the different ILs in the boundary regime do not correlate with the respective friction *coefficients* (*c.f.* Table 1). Had there been a correlation, it would have suggested that a single dissipation mechanism were operating in both regimes. As it is, different mechanisms must be responsible for the frictional dissipation in the two regimes, which is as expected. The sharp increase in lateral force occurs at slightly lower normal loads for some ILs (*e.g.*, PAF, PAN, and DMEAF) than for others (*e.g.*, EAF, EAN, and EtAN). This sharp increase is held to be a consequence of fluid dynamic effects and attractive interactions between the ion layers in the multilayer regime, where several ion layers separate the tip and the surface. At first glance, it seems possible that low friction might be a consequence of low IL viscosity, due to fluid dynamic effects associated with liquid motion about the probe. However, we have previously reported low friction for butylimidazolium iodide (viscosity ~ 1110 mPa·s) confined between a silica colloid probe

and a gold substrate,⁷³ so the explanation is clearly more complicated, as is the question of the value of the viscosity under confinement.³ The multilayer regime has been previously studied in some detail by us⁵⁴ and Perkin *et al.*⁴⁵⁻⁴⁸ The primary focus of this article is however the boundary region, and how ion structure influences lubricity.

At all forces in the boundary regime a single layer of ions separates the probe and substrate. Both mica and silica are negatively charged, but mica is expected to have a higher charge than silica in an IL⁴ so more IL cation charged groups will orientate preferentially towards mica (time averaged). Anions are also expected to be present in the boundary layer, but at lower concentrations.⁵¹ Note that ions in the layer are dynamic, and can rotate,⁵⁵⁻⁵⁷ translate, and exchange with ions in the bulk.^{45, 52, 54}

In the boundary regime, near-surface multilayers of IL are expelled ahead of the sliding contact such that a single ion layer remains. Multilayer expulsion has an energetic cost due to attractive interactions between the boundary layer and near surface layers being disrupted. Thus, the two broad pathways available for dissipation as the probe slides are via the ions in the boundary layer, and expulsion of multilayers during sliding. The amount of energy dissipated through either pathway is dependent on the strength of the interactions between the ions, and therefore the IL species. This is different from the multilayer regime where dissipation is primarily a consequence of several IL layers sliding over one another.⁴⁸

Friction forces at the start of the boundary regime are higher for PAN and PAF than for EAN and EAF. This is because solvophobic interactions are stronger for the C₃ alkyl chains than C₂ alkyl chains, and thus the attractive interaction between boundary layer ions and near surface layers are stronger. More energy is thus required to strip away the near-surface IL layers from the boundary layer for C₃ cations, resulting in greater energy dissipation and friction. The friction coefficients for the multilayer regime in Table 1 reflect the strength of

attractions between the boundary layer and near surface layers, with stronger attractions producing higher friction coefficients, along with a contribution from the multilayers sliding over each other. Since the interfacial IL nanostructure is different to the bulk structure,² the interfacial liquid cohesion is not necessarily the same as the bulk.

In Figure 1, it can also be observed that PAN and PAF display essentially identical behaviour as do EAN and EAF. Thus, for the same cation, the nature of the anion has negligible effect on friction. Once again, this suggests that the dominant contribution to friction during the multilayer stripping is overcoming the solvophobic interaction with the boundary film and is not sensitive to the structure of the multilayers themselves. (Alternatively the formate ion and nitrate ion behave very similarly in terms of their contributions to the multilayer structure.) Furthermore the fact that the friction *coefficients* in the boundary regime are so similar implies either that the anions in the boundary films are “buried” within the film, or that during sliding their population in the boundary film is low.^{51, 52} Both the surfaces are intrinsically negatively charged, so for reasons of charge neutrality few anions would be expected.

The alcohol group of EtAN provides an additional hydrogen binding site compared to the EA⁺ and PA⁺ cations, producing a denser hydrogen bond network⁴³ which renders EtAN more cohesive than EAN and EAF. The alcohol group also disrupts the solvophobic interactions,⁴⁰ which play a dominant role in the structuring and ordering at surfaces and under confinement. This results in the friction force at the beginning of the boundary regime for EtAN being between that of the EA⁺ and PA⁺ ILs.

The force at the beginning of the boundary regime is lowest for DMEAF. This is because steric effects in DMEAF weaken solvophobic attractions¹¹ and branched groups pack less effectively in near surface layers,⁷⁴ allowing them to be more easily displaced.

In the boundary regime, the friction coefficients for PAN, PAF, EAN and EAF are all the same within error at ~ 1.1 , while EtAN is lower at 0.80 and DMEAF lowest at 0.57. During sliding over the cation alkyl chains, the dissipation pathways available are expected to be chain tilting, twisting, rotating, and gauche defect formation.⁵⁵⁻⁵⁷ The friction coefficient is lowest for DMEAF because the added methyl groups sterically hinder dissipation pathways, and only the methyl groups can rotate. The friction coefficient for EtAN is lower than for the *n*-alkane ammonium ILs because hydrogen bonds between cation alcohol groups in the boundary layer make it resistant to deformations and rotations.

It is somewhat surprising that the friction coefficients for EA⁺ and PA⁺ ILs are the same, because for self-assembled monolayers (SAMs)^{56, 57, 62} friction coefficients are lower for longer alkyl chains. For SAMs, as the alkyl chain length is increased the strength of lateral vdW's interactions between chains increases, creating a smoother, more robust sliding plane and lowering friction. For these ILs, increasing the alkyl chain from C₂ to C₃ does not increase the strength of lateral vdW's interactions enough to have a measurable effect – in general 6 carbons are considered necessary to achieve a self-assembly structure, at least in aqueous media. As such, the similarity of the EA⁺ and PA⁺ friction coefficients indicates that there are negligible differences in the energy dissipation within the boundary layer. It may well support the argument that a frictional mechanism is rearrangements in the position of the positive charge with respect to the mica surface engendered by the proximity of the silica surface, as argued earlier.⁷³

Figure 2 shows lateral force as a function of sliding velocity and load for EAF, PAF, DMEAF and EtAN. The corresponding normal force curve is shown on a common load abscissa to allow the beginning of the boundary regime to be identified. The lateral force associated with the multilayer stripping increases with sliding velocity for each IL because of the viscous nature of the process, which leads to higher dissipation and friction. Similar data for EAN⁵⁴

and PAN⁵² have been published previously so are not presented. However, Figure 1 shows a similar, striking, lack of anion dependence for EA⁺ and PA⁺.

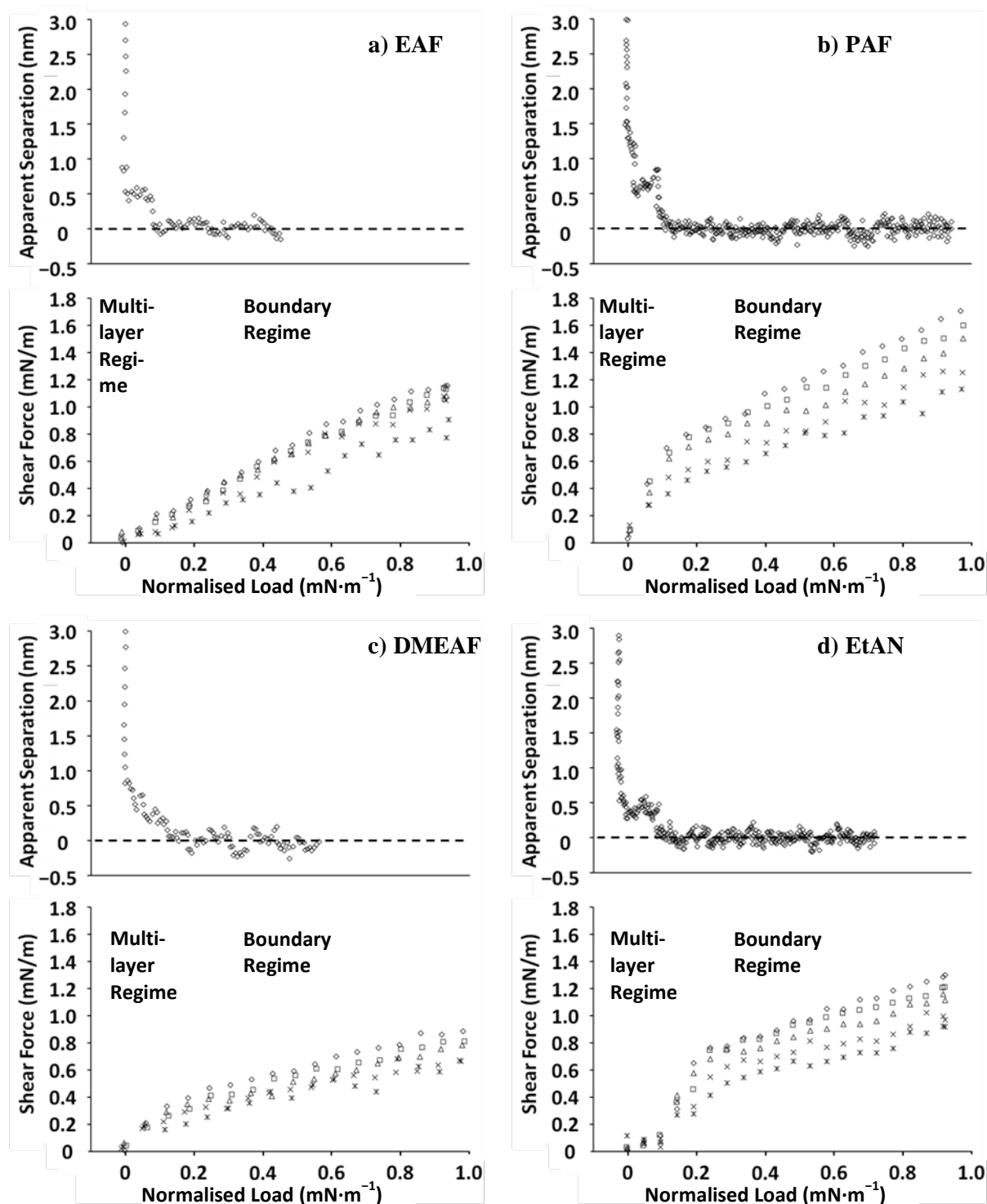


Figure 2. (top panels) Apparent separation between a mica surface and a silica colloid probe as a function of normal load in a) EAF, b) PAF, c) DMEAF, and d) EtAN. (bottom panels) Shear force as a function of normal load for various sliding velocities using a silica colloid probe. Diamonds: 40 $\mu\text{m}\cdot\text{s}^{-1}$, squares: 30 $\mu\text{m}\cdot\text{s}^{-1}$, triangles: 20 $\mu\text{m}\cdot\text{s}^{-1}$, crosses: 10 $\mu\text{m}\cdot\text{s}^{-1}$, stars: 5 $\mu\text{m}\cdot\text{s}^{-1}$. The dashed vertical lines delineate the multilayer regime from the boundary regime (see discussion).

Figure 3 plots the multilayer and boundary regime friction coefficients for the data presented in Figure 2. The form of the data in Figure 3 is similar to that obtained previously for EAN, and it is analysed in the same way,⁵⁴ while friction coefficients as a function of velocity for PAN have not been reported previously, so are shown in Figure 3. (The raw shear force versus normal load data for sliding velocities from $5 \mu\text{m}\cdot\text{s}^{-1}$ to $40 \mu\text{m}\cdot\text{s}^{-1}$ for PAN are shown in Figure K of the Supporting Information).

In the boundary layer regime, within the error of the measurement, the friction coefficient is independent of sliding velocity (or weakly increasing) over the range of sliding velocities accessed, c.f. Figure 3, right. An effective friction coefficient can also be extracted for the multilayer regime, though a certain degree of caution should be exercised since the transition from multi- to boundary layer occurs over this load range. The effective friction coefficient varies logarithmically with sliding velocity. Such a logarithmic response is usually a consequence of an activated, discontinuous sliding process, and has been observed previously for molecular liquids⁷⁵ and Langmuir-Blodgett films.⁷⁶ Fits to the multilayer friction coefficient data (Figure 3, left) are obtained using $\mu = \mu_0 + \alpha \times \ln(v)$ where the fitting constants μ_0 and α are liquid specific and related to the material process constants.⁷⁵ The values for μ_0 and α for each PIL are presented in Table 2.

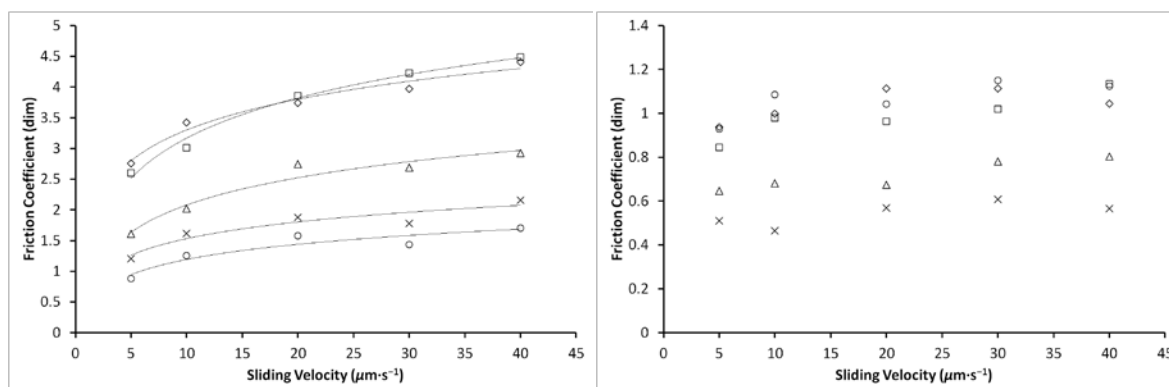


Figure 3. Multilayer regime effective friction coefficients (left) and boundary regime friction coefficients (right) for PAF, PAN, EtAN, EAF, and DMEAF as a function of sliding velocity for a silica colloid probe sliding against a mica surface. The effective friction coefficients in the left panel are taken over the range of loads from 0 to $\approx 0.2 \text{ mN}\cdot\text{m}^{-1}$. The solid lines in the left figure are logarithmic fits to the data. Squares: PAF, diamonds: PAN, triangles: EtAN, circles: EAF, crosses: DMEAF.

Table 2. μ_0 and α values for fits to the friction coefficients (μ) at various speeds for the multilayer regime using $\mu = \mu_0 + \alpha \times \ln(v)$.

Protic IL	μ_0	α
PAN	1.6	0.72
PAF	0.99	0.95
EtAN	0.59	0.64
DMEAF	0.62	0.40
EAF	0.37	0.35

Logarithmic friction – velocity relationships result from a discontinuous sliding process⁷⁷ when the sliding velocity is comparable to the material intrinsic relaxation times.⁷⁵ In nanotribological systems, sliding discontinuities are caused by stick-slip like processes at, or near, molecular length scales in a Tomlinson-like fashion.^{78, 79} Here the harmonic potentials correspond to the effective spring constants of the interfacial molecules (or ions). Such models have been successfully used to model confined polymers,⁷⁶ crystals,⁸⁰ and molecular liquids.⁷⁵ The value of α (Table 2) is *inversely* proportional to the coherence length of the

process; the length over which the system is able to store strain before sliding. Thus, the ILs with the smallest α values have the largest coherence lengths. This suggests that EAF and DMEAF possess the largest coherence lengths, EtAN is intermediate, while PAN and PAF are shortest. This trend is in good agreement with the levels of liquid cohesion in near surface multilayers, which are expected to be highest for PAF and PAN (C_3 alkyl chain produces strong solvophobic attraction), weak for EAF and DMEAF (short alkyl chain / steric hindrance produces a weaker solvophobic attraction) and intermediate for EtAN due to the extra H-bond donor/acceptor site derived from the added alcohol group.

The friction coefficient in the boundary regime is smaller than that determined for the multilayer regime and independent of sliding velocity within experimental error. This shows that the molecular time scales causing dissipation are fast compared to the sliding velocities being employed consistent with the idea of sliding on a single layer of ions where rotations and molecular rearrangement are the only dissipative mechanisms. The fact that this is not the case for the multilayer regime is due to the fact that the slipping events are caused by the collective movement of many ion pairs and even layers.

Conclusions

Friction Force Microscopy (FFM) has been used to elucidate the impact of protic ionic liquid (IL) molecular structure on the nano-scale friction of six protic ILs confined between a silica colloid probe and a mica surface. For all ILs, at low force multiple ion layers are present between the probe and the surface. Friction is low, but the effective coefficient in this region is rather large and energy is dissipated mainly through the ion layers sliding over each other.

After the threshold force of the boundary regime is exceeded, a single layer of ions separates the probe and the surface during sliding. Under these conditions, energy is dissipated in two main ways: (i) by expulsion of near surface IL multilayers from the space between the tip and the surface (largely load independent) and (ii) deformations and rotations of ions in the boundary layer. For (i), friction is higher when attractive interactions between ions in near surface layers are stronger, because more energy is required to expel the layers from between the tip and surface. Such attraction can result from longer alkyl chains producing a stronger solvophobic effect (for PA⁺ ILs) or additional hydrogen bonding groups (for EtAN). The interactions within and between layers can be controlled by introducing steric hindrance as is the case with DMEA⁺ or additional hydrogen bonding as with EtA⁺.

For a given cation, the anion species is of little consequence for the frictional properties, which strongly supports the argument of the boundary layer being cation-rich. This is probably a result of the experimental system being composed of two intrinsically negatively charged surfaces. This hypothesis could for example be tested by the use of two oppositely charged surfaces, or by controlling the surface potential of one of the surfaces.

The effect of increasing sliding velocity has been probed. As the surfaces slide faster, more energy is imparted to the system, and is dissipated *via* the dominate pathway for a particular IL. Over the range of velocities the boundary layer friction coefficients did not change (within error) meaning that new energy pathways have not become available.

Acknowledgements

This research was supported by an ARC Discovery Project (DP120102708) and an ARC Future Fellowship (FT120100313) for RA. JS thanks Dr Oliver Werzer for development of

and permission to use the computer program used for data analysis. Dr Hua Li and Mr Robert Hayes are thanked for helpful discussions. MR acknowledges support from the Swedish Research Council, the Strategic Research Foundation SSF, and ILEAP-financed by K&A Wallenberg Foundation.

Supporting Information Available

Normal force curves and shear force as a function of normal load for velocities from $5 \mu\text{m}\cdot\text{s}^{-1}$ to $30 \mu\text{m}\cdot\text{s}^{-1}$ for all ILs are presented in the supporting information. This information is available free of charge *via* the Internet at <http://pubs.rsc.org/en/journals>.

References

1. T. Welton, *Chem. Rev.*, 1999, **99**, 2071-2083.
2. R. Hayes, G. G. Warr and R. Atkin, *Phys. Chem. Chem. Phys.*, 2010, **12**, 1709-1723.
3. R. A. Asencio, E. D. Cranston, R. Atkin and M. W. Rutland, *Langmuir*, 2012, **28**, 9967-9976.
4. R. Atkin and G. G. Warr, *J. Phys. Chem. C*, 2007, **111**, 5162-5168.
5. W. L. Hough and R. D. Rogers, *Bull. Chem. Soc. Jpn.*, 2007, **80**, 2262-2269.
6. D. Wakeham, PhD Thesis, University of Newcastle, 2012.
7. T. J. Geldbach and P. J. Dyson, *J. Am. Chem. Soc.*, 2004, **126**, 8114-8115.
8. J. A. Smith, O. Werzer, G. B. Webber, G. G. Warr and R. Atkin, *J. Phys. Chem. Lett.*, 2010, **1**, 64-68.
9. S. Z. El Abedin, P. Giridhar, P. Schwab and F. Endres, *Electrochem. Comm.*, 2010, **12**, 1084-1086.
10. R. Atkin, S. Z. El Abedin, R. Hayes, L. H. S. Gasparotto, N. Borisenko and F. Endres, *J. Phys. Chem. C*, 2009, **113**, 13266-13272.
11. D. Wakeham, R. Hayes, G. G. Warr and R. Atkin, *J. Phys. Chem. B*, 2009, **113**, 5961-5966.
12. P. Niga, D. Wakeham, A. Nelson, G. G. Warr, M. Rutland and R. Atkin, *Langmuir*, 2010, **26**, 8282-8288.
13. D. Wakeham, P. Niga, G. G. Warr, M. W. Rutland and R. Atkin, *Langmuir*, 2010, **26**, 8313-8318.
14. J. W. Choi, G. Cheruvally, Y. H. Kim, J. K. Kim, J. Manuel, P. Raghavan, J. H. Ahn, K. W. Kim, H. J. Ahn, D. S. Choi and C. E. Song, *Solid State Ionics*, 2007, **178**, 1235-1241.
15. M. Gratzel, *Nature*, 2001, **414**, 338-344.
16. M. U. Araos and G. G. Warr, *J. Phys. Chem. B*, 2005, **109**, 14275-14277.
17. M. U. Araos and G. G. Warr, *Langmuir*, 2008, **24**, 9354-9360.
18. R. Atkin, S. M. C. Bobillier and G. G. Warr, *J. Phys. Chem. B*, 2010, **114**, 1350-1360.
19. R. Atkin and G. G. Warr, *J. Am. Chem. Soc.*, 2005, **127**, 11940-11941.
20. T. L. Greaves and C. J. Drummond, *Chem. Soc. Rev.*, 2008, **37**, 1709-1726.
21. H. Rodriguez and R. D. Rogers, *Fluid Phase Equilib.*, 2010, **294**, 7-14.

22. D. Jiang, L. T. Hu and D. P. Feng, *Tribol. Lett.*, 2011, **41**, 417-424.
23. J. Sweeney, F. Hausen, R. Hayes, G. B. Webber, F. Endres, M. W. Rutland, R. Bennewitz and R. Atkin, *Phys. Rev. Lett.*, 2012, **109**, 5.
24. A. E. Somers, S. M. Biddulph, P. C. Howlett, J. Z. Sun, D. R. MacFarlane and M. Forsyth, *Phys. Chem. Chem. Phys.*, 2012, **14**, 8224-8231.
25. A. E. Somers, P. C. Howlett, J. Sun, D. R. MacFarlane and M. Forsyth, *Tribol. Lett.*, 2010, **40**, 279-284.
26. A. E. Somers, P. C. Howlett, J. Sun, D. R. MacFarlane and M. Forsyth, *Phosphonium ionic liquids as lubricants for aluminium-steel*, Wit Press, Southampton, 2010.
27. A. E. Somers, B. Khemchandani, P. C. Howlett, J. Z. Sun, D. R. MacFarlane and M. Forsyth, *ACS Appl. Mater. Interfaces*, 2013, **5**, 11544-11553.
28. B. Kinzig, P. Sutor, G. W. Sawyer, A. Rennie, P. Dickrell and J. Gresham, in *World Tribology Congress*, Washington DC, USA, 2005, pp. 509-510.
29. D. M. Li, M. R. Cai, D. P. Feng, F. Zhou and W. M. Liu, *Tribol. Int.*, 2011, **44**, 1111-1117.
30. X. Liu, F. Zhou, Y. Liang and W. Liu, *Tribol. Lett.*, 2006, **23**, 191-196.
31. B. S. Phillips and J. S. Zabinski, *Tribol. Lett.*, 2004, **17**, 533-541.
32. J. B. Pu, L. P. Wang, Y. F. Mo and Q. J. Xue, *J. Colloid Interf. Sci.*, 2011, **354**, 858-865.
33. F. Zhou, Y. M. Liang and W. M. Liu, *Chem. Soc. Rev.*, 2009, **38**, 2590-2599.
34. W. M. Liu, C. F. Ye, Q. Y. Gong, H. Z. Wang and P. Wang, *Tribol. Lett.*, 2002, **13**, 81-85.
35. M. Palacio and B. Bhushan, *Ultramicroscopy*, 2009, **109**, 980-990.
36. F. U. Shah, S. Glavatskih and O. N. Antzutkin, *Tribol. Lett.*, 2013, **51**, 281-301.
37. F. U. Shah, S. Glavatskih, D. R. MacFarlane, A. Somers, M. Forsyth and O. N. Antzutkin, *Phys. Chem. Chem. Phys.*, 2011, **13**, 12865-12873.
38. C. F. Ye, W. M. Liu, Y. X. Chen and L. G. Yu, *Chem. Commun.*, 2001, 2244-2245.
39. B. Bhushan, M. Palacio and B. Kinzig, *J. Colloid Interf. Sci.*, 2008, **317**, 275-287.
40. R. Hayes, S. Imberti, G. G. Warr and R. Atkin, *Phys. Chem. Chem. Phys.*, 2011, **13**, 3237-3247.
41. R. Hayes, S. Imberti, G. G. Warr and R. Atkin, *Phys. Chem. Chem. Phys.*, 2011, **13**, 13544-13551.
42. R. Hayes, S. Imberti, G. G. Warr and R. Atkin, *Angew. Chem.-Int. Edit.*, 2012, **51**, 7468-7471.
43. R. Hayes, S. Imberti, G. G. Warr and R. Atkin, *Angew. Chem.-Int. Edit.*, 2013, **52**, 4623-4627.
44. R. G. Horn, D. F. Evans and B. W. Ninham, *J. Phys. Chem.*, 1988, **92**, 3531-3537.
45. S. Perkin, T. Albrecht and J. Klein, *Phys. Chem. Chem. Phys.*, 2010, **12**, 1243-1247.
46. S. Perkin, L. Crowhurst, H. Niedermeyer, T. Welton, A. M. Smith and N. N. Gosvami, *Chem. Commun.*, 2011, **47**, 6572-6574.
47. A. M. Smith, K. R. J. Lovelock, N. N. Gosvami, P. Licence, A. Dolan, T. Welton and S. Perkin, *J. Phys. Chem. Lett.*, 2013, **4**, 378-382.
48. A. M. Smith, K. R. J. Lovelock, N. N. Gosvami, T. Welton and S. Perkin, *Phys. Chem. Chem. Phys.*, 2013, **15**, 15317-15320.
49. R. Atkin, N. Borisenko, M. Druschler, S. Z. El Abedin, F. Endres, R. Hayes, B. Huber and B. Roling, *Phys. Chem. Chem. Phys.*, 2011, **13**, 6849-6857.
50. R. Hayes, N. Borisenko, M. K. Tam, P. C. Howlett, F. Endres and R. Atkin, *J. Phys. Chem. C*, 2011, **115**, 6855-6863.
51. J. J. Segura, A. Elbourne, E. J. Wanless, G. G. Warr, K. Voitchovsky and R. Atkin, *Phys. Chem. Chem. Phys.*, 2013, **15**, 3320-3328.
52. A. Elbourne, J. Sweeney, G. B. Webber, E. J. Wanless, G. G. Warr, M. W. Rutland and R. Atkin, *Chem. Commun.*, 2013, **49**, 6797-6799.
53. A. Ray, *Nature*, 1971, **231**.
54. O. Werzer, E. D. Cranston, G. G. Warr, R. Atkin and M. W. Rutland, *Phys. Chem. Chem. Phys.*, 2012, **14**, 5147-5152.
55. M. Salmeron, *Tribol. Lett.*, 2001, **10**, 69-79.
56. N. J. Brewer, B. D. Beake and G. J. Leggett, *Langmuir*, 2001, **17**, 1970-1974.

57. N. J. Brewer, T. T. Foster, G. J. Leggett, M. R. Alexander and E. McAlpine, *J. Phys. Chem. B*, 2004, **108**, 4723-4728.
58. V. N. Bliznyuk, M. P. Everson and V. V. Tsukruk, *J. Tribol.-Trans. ASME*, 1998, **120**, 489-495.
59. M. Porto, M. Urbakh and J. Klafter, *J. Phys. Chem. B*, 2000, **104**, 3791-3794.
60. M. Ruths, *J. Phys. Chem. B*, 2006, **110**, 2209-2218.
61. M. Ruths, S. Lundgren, K. Danerlov and K. Persson, *Langmuir*, 2008, **24**, 1509-1516.
62. X. D. Xiao, J. Hu, D. H. Charych and M. Salmeron, *Langmuir*, 1996, **12**, 235-237.
63. A. Lio, D. H. Charych and M. Salmeron, *J. Phys. Chem. B*, 1997, **101**, 3800-3805.
64. T. L. Greaves, A. Weerawardena, I. Krodkiewska and C. J. Drummond, *J. Phys. Chem. B*, 2008, **112**, 896-905.
65. E. Liu, B. Blanpain and J. P. Celis, *Wear*, 1996, **192**, 141-150.
66. U. D. Schwarz, P. Koster and R. Wiesendanger, *Rev. Sci. Instrum.*, 1996, **67**, 2560-2567.
67. W. A. Ducker, T. J. Senden and R. M. Pashley, *Nature*, 1991, **353**, 239-241.
68. J. Ralston, I. Larson, M. W. Rutland, A. A. Feiler and M. Kleijn, *Pure Appl. Chem.*, 2005, **77**, 2149-2170.
69. J. E. Sader, J. W. M. Chon and P. Mulvaney, *Rev. Sci. Instrum.*, 1999, **70**, 3967-3969.
70. C. P. Green, H. Lioe, J. P. Cleveland, R. Proksch, P. Mulvaney and J. E. Sader, *Rev. Sci. Instrum.*, 2004, **75**, 1988-1996.
71. B. Derjaguin, *Kolloid Z*, 1934, **69**, 155-164.
72. R. Hayes, S. Z. El Abedin and R. Atkin, *J. Phys. Chem. B*, 2009, **113**, 7049-7052.
73. H. Li, R. J. Wood, M. W. Rutland and R. Atkin, *Chem. Commun.*, 2014, **50**, 4368-4370.
74. S. T. Cui, P. T. Cummings and H. D. Cochran, *J. Chem. Phys.*, 2001, **114**, 6464-6471.
75. M. He, A. Szuchmacher Blum, G. Overney and R. M. Overney, *Phys. Rev. Lett.*, 2002, **88**, 154302.
76. T. Bouhacina, J. P. Aime, S. Gauthier, D. Michel and V. Heroguez, *Phys. Rev. B*, 1997, **56**, 7694-7703.
77. B. J. Briscoe and D. C. B. Evans, *Proc. R. Soc. London Ser. A-Math. Phys. Eng. Sci.*, 1982, **380**, 389-407.
78. L. Prandtl, *Z. Angew. Math. Mech.*, 1928, **8**.
79. G. A. Tomlinson, *Philos. Mag.*, 1929, **7**, 905-939.
80. E. Gnecco, R. Bennewitz, T. Gyalog, C. Loppacher, M. Bammerlin, E. Meyer and H. J. Guntherodt, *Phys. Rev. Lett.*, 2000, **84**, 1172-1175.

